

Optimisation of the *Swift* X-ray follow-up of Advanced LIGO and Virgo gravitational wave triggers in 2015–16

P.A. Evans^{1*}, J.P. Osborne¹, J.A. Kennea², S. Campana³ P.T. O’Brien¹,
N.R. Tanvir¹, J.L. Racusin⁴, D.N. Burrows², S.B. Cenko^{4,5}, N. Gehrels⁴

¹*Department of Physics and Astronomy, University of Leicester, Leicester, LE1 7RH, UK*

²*Department of Astronomy and Astrophysics, Pennsylvania State University, 525 Davey Lab, University Park, PA 16802, USA*

³*INAF – Osservatorio Astronomico di Brera, via E. Bianchi 46, I-23807, Merate, Italy*

⁴*Astrophysics Science Division, NASA Goddard Space Flight Center, Mail Code 661, Greenbelt, MD 20771, USA*

⁵*Joint Space-Science Institute, University of Maryland, College Park, MD 20742, USA*

Accepted – Received –

ABSTRACT

One of the most exciting near-term prospects in physics is the potential discovery of gravitational waves by the advanced LIGO and Virgo detectors. To maximise both the confidence of the detection and the science return, it is essential to identify an electromagnetic counterpart. This is not trivial, as the events are expected to be poorly localised, particularly in the near-term, with error regions covering hundreds or even thousands of square degrees. In this paper we discuss the prospects for finding an X-ray counterpart to a gravitational wave trigger with the *Swift* X-ray Telescope, using the assumption that the trigger is caused by a binary neutron star merger which also produces a short gamma-ray burst. We show that it is beneficial to target galaxies within the GW error region, highlighting the need for substantially complete galaxy catalogues out to distances of 300 Mpc. We also show that nearby, on-axis short GRBs are either extremely rare, or are systematically less luminous than those detected to date. We consider the prospects for detecting afterglow emission from an off-axis GRB which triggered the GW facilities, finding that the detectability, and the best time to look, are strongly dependent on the characteristics of the burst such as circumburst density and our viewing angle.

Key words:

1 INTRODUCTION

In the last quarter of 2015 the Advanced LIGO observatory (ALIGO; Harry et al. 2010) is expected to begin its first science run, spending three months searching for gravitational waves (GW). In 2016 it will be joined by Advanced Virgo (AVirgo; Acernese et al. 2015), and perform a six-month long run (LIGO Scientific Collaboration et al. 2013). Electromagnetic (EM) follow-up of GW triggers is essential to maximise the scientific information gleaned from any such detection, as well as providing a useful confirmation of the GW signal. To this end, much effort is currently being expended both in predicting what EM signal will accompany a GW event (e.g. Metzger & Berger 2012; Andersson et al. 2013), and in planning observational follow-up strategies (e.g. Nissanke, Kasliwal & Georgieva 2013). Of course, this depends on what gives rise to the GW signal in the

ALIGO/Virgo bandpass. While various phenomena (e.g. core-collapse supernovae, magnetar flares) are expected to give rise to GW signals, the most promising phenomenon is believed to be the merger of two stellar mass compact objects such as neutron stars (NS) or black holes. The final stages of such a merger are expected to emit a GW ‘chirp’ that could be detected by ALIGO/AVirgo, if the event is near enough to Earth. The predicted rates of such mergers that will be detectable with ALIGO/AVirgo is highly uncertain, with estimates (e.g. Abadie et al. 2010; Coward et al. 2012) covering up to 4 orders of magnitude! Electromagnetically, such a merger is accompanied by a range of emission (see Metzger & Berger 2012) including that of a short gamma-ray burst (sGRB). These are short ($\lesssim 2$ s) but extremely intense ($L \sim 10^{51}$ erg s⁻¹) flashes of high energy radiation, followed by a panchromatic ‘afterglow’ from the shocked circumstellar material; see Berger (2014) for a review. The marriage of EM and GW signals from an sGRB is extremely valuable as the mass, distance and bi-

* pae9@leicester.ac.uk

nary inclination information potentially available from the GW signal complements the luminosity, redshift and duration measurements available from EM observations to constrain accurately the energetics and hence physics of the merger process. These measurements also have the potential to constrain cosmology, through combining GW distance information with spectroscopic redshifts (e.g. Schutz 1986; Nissanke et al. 2010). Additionally, a precise EM location should permit the identification of the host galaxy and source environment.

In this paper we consider how best to respond to GW triggers with the *Swift* satellite (Gehrels et al. 2004). We are only considering the case that the GW event is accompanied by an sGRB, and we assume that the sGRB arose from an NS-NS merger, i.e. we do not consider NS-BH mergers. This is primarily because the input to our work are the GW simulations of Singer et al. (2014), who simulated the GW signal from NS-NS systems. The main consequence of this is that we may be underestimating the typical distance of the GW triggers, since NS-BH binaries can be detected out to greater distance than the NS-NS binaries (e.g. LIGO Scientific Collaboration et al. 2013). *Swift* was designed to study GRBs and, at the time of writing, the on-board Burst Alert Telescope (BAT; Barthelmy et al. 2005) has detected nearly 1,000, including ~ 85 sGRBs¹, and localised them to within $3'$ at trigger time. Of those bursts which were promptly observed by the narrow field, 0.3–10 keV X-ray telescope (XRT; Burrows et al. 2005) almost all (94% of all GRBs, 80% of short GRBs) have been detected and around 40% were detected by the UV/optical telescope (UVOT; Roming et al. 2005). *Swift*-BAT has a peak sensitivity at a significantly lower energy than *CGRO*-BATSE and *Fermi*-GBM and -LAT, which disfavors the detection of sGRBs (the fraction of *Swift*-triggered GRBs that are short is much lower than for these other missions). However, very nearby events, such as expected as GW detections, are likely to be bright in gamma-rays and largely unaffected by this bias. A more significant issue is the BAT's constrained field of view (2 sr, i.e. $\sim \frac{1}{6}$ of the sky) which means that it is rather unlikely that an sGRB which triggers ALIGO/AVirgo will also trigger the BAT (this is without considering the question of whether typical mergers are likely to produce bright sGRBs, which we discuss in Section 7). Therefore, in order to localise the sGRB with *Swift* we will need to rely on follow-up with the narrow-field instruments. In this work we focus on the XRT, since it has detected almost every GRB it has looked for; and, as we will demonstrate in Section 2.1, the rate of 'contaminating' X-ray transients unrelated to the GW trigger is much lower than at optical wavelengths.

While the BAT GRB localisation fits easily inside the XRT field of view (radius $12.3'$); for GW events the error region will likely cover many hundreds of square degrees (e.g. Nissanke, Kasliwal & Georgieva 2013; Singer et al. 2014; Berry et al. 2015). *Swift* not only has the ability to slew rapidly, but it can also autonomously perform multiple overlapping 'tiled' observations (Evans et al. 2015), allowing it to cover large error regions, although this has not yet been attempted for regions as large as expected from ALIGO/AVirgo. *Swift* has previously observed the fields of

two GW triggers (Evans et al. 2012), but these observations were extremely limited, covering less than one square degree between the two triggers. Kanner et al. (2012) explored ways of observing the large GW error regions with XRT, and suggested that, initially, XRT should observe a subset of nearby galaxies in the GW error region. When the GW horizon distance increases, they suggest observing a series of tiled pointings, of 100 s each. Despite this work, it is not obvious what the *optimal* means of observing the ALIGO/Virgo error region with the *Swift*-XRT is, both in terms of where to look, and how long to look for. In this paper we use end-to-end simulations to explore the optimal approach to following up GW triggers with *Swift*-XRT, under the assumption that the underlying event is a NS-NS merger accompanied by an sGRB.

2 HOW TO IDENTIFY THE X-RAY AFTERGLOW

As noted by authors such as Metzger & Berger (2012), when responding to triggers such as those from ALIGO/AVirgo, we do not simply need to detect the EM counterpart, but also to identify it as such, from among the unrelated sources detected. Evans et al. (2015) proposed two ways of distinguishing an X-ray GRB afterglow from unrelated, uncatalogued sources using *Swift*: brightness or fading behaviour. If a source is bright enough that it should have been catalogued, but is not, then it is by definition some form of transient phenomenon, and could be the afterglow. Alternatively, GRB afterglows are known to fade on short timescales, therefore an uncatalogued and fading object is also a good candidate afterglow, even if it is not above the catalogue limit. However, GRBs are not the only transient phenomena in the X-ray sky, and when observing the large GW error regions we need to consider the possibility of coincidentally detecting a transient, unrelated to the GW signal, which we now do.

2.1 False alarm rates

To investigate the rate of bright X-ray transients, we selected all GRB datasets (apart from stacked images) from the 1SXPS catalogue (Evans et al. 2014), which gives position and flux (among other things) for all point sources observed by XRT up to 2012 October. We limited ourselves to the GRB fields as, in these cases, which X-ray source was the target of the observation is known, so cannot be mistaken for a serendipitous or unrelated object. Within each of these fields, we searched for X-ray sources which were not the GRB, were not catalogued X-ray emitters², had a detection flag of *Good*, *Reasonable* or *Poor*, and were brighter than a $3\text{-}\sigma$ upper limit from the *Rosat* All Sky Survey (RASS; Voges et al. 1999), calculated at the location of the source (see Section 3 for details of the RASS upper limit determination). That is, we selected all objects which would trigger our 'bright source' criterion but lie coincidentally in the XRT

¹ Defined here naively as simply those with $T_{90} \leq 2$ s.

² Unless the catalogue entry was from one of the earlier XRT catalogues, i.e. detected in the same dataset as in the 1SXPS catalogue.

field of view. We found 32 such objects, in a total of 52.6 Ms of observing time, covering ~ 95 square degrees on the sky.

To infer the rate of these transients requires knowledge of their duration. If they are all short-lived (compared to the typical duration of an XRT exposure, ~ 500 s) then the rate at which X-ray transients ‘turn-on’ is 1 per 1.64 Ms per XRT field of view (0.12 square degrees). The observing strategies explored later in this paper cover XRT exposure times of 0.006–1 Ms per GW trigger; with those defined as ‘best’ (see Section 5.1–5.2) requiring 0.03–0.18 Ms per trigger. So, for each GW trigger we follow with XRT, this predicts a ~ 2 –10% chance of detecting a bright X-ray transient unrelated to the GW trigger. This is much lower than the expected rates of optical transients, which could be as high as hundreds of events per GW trigger (e.g. Nissanke, Kasliwal & Georgieva 2013, although see, e.g., Cowperthwaite & Berger 2015 for ways to mitigate this). It is also an upper limit, since the 1SXPS observations from which it was derived are of sufficient exposure to detect all sources above the RASS limit, whereas, for most strategies explored in Section 3 the exposures are much shorter than this, so most of the 32 bright sources in 1SXPS would not be detected.

On the other hand, if the transients last long enough to all be ‘active’ at the same time (~ 5 –10 years), then we have determined that transients exist on the sky with a density of 0.3 per square degree. The strategies we will explore in this work cover 6–216 square degrees, thus we would predict ~ 2 –65 transients unrelated to the GW event to be detected by our observations. The reality is likely somewhere between these two values. The *Swift* data do not allow us to place strong constraints on the duration of the 32 transient events as, in all but 9 cases, the transient was either already above the RASS limit when XRT first observed it, or still above the limit when XRT stopped observing it. For the 9 cases where both the start and end of the transient phase were seen by XRT, the median duration is $\sim 2 \times 10^5$ s. This is short compared to the time interval over which the 32 transients were detected (250 Ms), so we suggest that the false positive rate is likely to be closer to the first value (one per XRT field of view per 1.64 Ms) than the second one (0.3 per square degree).

Kanner et al. (2013) have also investigated the expected rate of X-ray transients, based on *XMM-Newton* Slew Survey data. It is difficult to directly compare their results with ours, since they used different selection criteria (using only the 0.2–2 keV band, selecting sources with a flux $10\times$ the RASS $2\text{-}\sigma$ upper limit, and only those associated with known galaxies) which will detect fewer transients than our approach. They also only gave the spatial density of transients, with no temporal information. However, they predict that the probability of XRT detecting a transient unrelated to a GW trigger in observations covering 35 deg^2 and of 100 s each, is $\lesssim 1\%$. If we assume one transient per XRT field of view, per 1.64 Ms, we predict 1.8%; these numbers are reasonably compatible, given the above differences in measurements, and supports our belief in the lower of the two false positive rates we have deduced.

To determine the rate at which fading X-ray sources unrelated to the GW event will be detected is more complicated, since it depends heavily on the observing strategy employed. However, we can gain an estimate of the rate from

Evans et al. (2015). In response to 20 neutrino triggers from IceCube, they detected a total of 72 sources in their initial XRT observations, of which only one initially appeared to be fading (further observations showed that it was not related to the neutrino trigger). Therefore we can place a crude estimate that $\sim 1/72=1.4\%$ of objects detected by XRT but not related to the GW trigger will show fading behaviour.

These considerations demonstrate that, if a candidate counterpart to the GW event is detected in X-rays, the probability of it being unrelated to the GW trigger is relatively small. Additionally, since *Swift* is in space with a 96-min orbit, and only a 46° -radius exclusion zone around the Sun and 22° zone around the Moon, it can observe a much larger fraction of the sky (and hence GW error region) than a ground-based facility. This shows that *Swift*-XRT is a potentially valuable resource in searching for the EM counterpart to a GW trigger.

2.2 Feasibility and strategy

The size of the GW error regions (hundreds of square degrees) makes observing them a challenge for the narrow-field XRT on *Swift*; therefore it is necessary to observe a large number of ‘fields’: that is, distinct (but possibly overlapping) locations on the sky. To determine the optimal strategy for observing these fields there are two chief questions which need investigating. The first is whether to select XRT fields to cover the raw error region produced by ALIGO, or to target specific locations within it. With its modest field of view, XRT cannot in most cases, expect to cover the entire GW error region within a reasonable time after the trigger. The simplest approach is, if we can observe N XRT fields, to select the N fields which enclose the most probability (this is the concept of ‘searched area’ in Singer et al. 2014). However, sGRBs are expected to exist in or near to galaxies (e.g. Fong, Berger & Fox 2010; Tunnicliffe et al. 2014), therefore it may actually be better to first convolve the ALIGO probability map with an appropriate galaxy catalogue, and observe the most probable N fields after this convolution: this is the approach which was followed in earlier *Swift* follow-up of LIGO-Virgo triggers (Evans et al. 2012), and was advocated by Kanner et al. (2012) and Nuttall & Sutton (2010) for nearby GW events. This approach has the advantage of dramatically reducing the area that has to be covered, and therefore reducing the average time from the GRB to when XRT observes it. On the other hand, galaxy catalogues are not complete, and therefore some fraction of the time, this approach will mean discarding the XRT field which actually contains the GRB.

The second question is for how long each field is observed. Longer observations³ allow fainter sources to be detected, however they also increase the time it takes to reach the field which contains the GRB. Since GRB X-ray afterglows fade, this increased delay between the GRB and the observation may make the GRB undetectable. Also, the longer the exposure, the more unrelated sources we expect to detect, making identifying the GRB a greater challenge (if we have to re-observe the sources to look for fading, then the

³ Here, and throughout, by ‘observation’ we mean a single exposure of a single field.

required observing time scales with the number of unrelated uncatalogued sources).

2.2.1 Galaxy Catalogues

To investigate the first question – whether or not it is better to preferentially observe fields containing known galaxies – we require a galaxy catalogue to use in our simulations. In this work we used the Gravitational Wave Galaxy Catalogue (GWGC; White, Daw & Dhillon 2011): a compilation of various pre-existing catalogues. This gives the position, distance, size and orientation of galaxies out to 100 Mpc. The ALIGO probability maps (Section 3) are in HEALPIX format (Górski et al. 2005), therefore we created a HEALPIX-format mask, based on the GWGC. Since NS are often given a ‘kick’ at the moment of their birth, and indeed sGRBs are often found significantly offset from their host (e.g. Fong, Berger & Fox 2010; Church et al. 2011), we added a 100 kpc halo to each galaxy further than 5 Mpc (for galaxies closer than this, the angular projection of a 100 kpc halo covers an unreasonably large fraction of the sky, but the fraction of binary NS mergers which occur within this distance is negligible); all pixels in the HEALPIX mask that lay within a galaxy or its halo were set to 1, the remaining pixels were set to 0.

The GWGC catalogue is not complete, however an estimate of its completeness (based on *B*-band luminosity) is given in fig. 5 of White, Daw & Dhillon (2011). Based on this figure we have tabulated the approximate completeness of the catalogue as a function of distance in Table 1. We interpolated within this table to determine the completeness of the GWGC at various distances throughout this paper. This completeness estimate is based on *B* magnitude, which is likely to be a reasonable indicator of sGRB rate since, as noted by Fong et al. (2013), sGRB “demographics are consistent with a short GRB rate driven by both stellar mass and star formation.” Therefore, the published GWGC completeness will give a useful indication of the value or otherwise of using galaxy catalogues in the follow-up of GW triggers.

A drawback to the GWGC is that it only extends to 100 Mpc, whereas in the 2016 science run, when both ALIGO and AVirgo are active, we expect to detect GW events from beyond this horizon (Singer et al. 2014). While alternative catalogues exist which do extend beyond 100 Mpc, e.g. the 2MASS Photometric Redshift Catalog (2MPZ; Bilicki et al. 2014) – which contains photometric redshifts for galaxies detected in the 2MASS infrared survey, with a median of $z = 0.08$ (~ 300 Mpc) – the completeness of these has not been quantified, and the redshifts are photometric, so we have not used these in our simulations.

3 SIMULATION PROCEDURE

In order to simulate the *Swift*-XRT follow-up of sGRBs which trigger ALIGO/AVirgo, and explore the impact of different observing strategies, we used the GW simulations of Singer et al. (2014). These authors simulated the GW emission from a large number of NS-NS mergers distributed homogeneously in space, produced the ALIGO/AVirgo signals which would be detected from these and applied the data

Table 1. Completeness of the GWGC, based on fig. 5 of White, Daw & Dhillon (2011).

Distance (Mpc)	Completeness (%)
≤ 40	100
50	70
60	65
70	65
80	60
90	58
100	55
>100	0 ^a

^a The GWGC only includes galaxies within 100 Mpc, hence the sudden cut-off.

analysis routines to those signals. This was done for the expected ALIGO configuration in 2015, and for the ALIGO-AVirgo configuration (and duty cycles) expected in 2016. For the mergers which were detected by this process, the probability map and the input binary system parameters, are available online⁴. We are only interested in the mergers which are accompanied by sGRBs, for which the jet of outflowing material is directed towards the Earth. The opening angle of sGRB jets is not well known (e.g. Margutti et al. 2012; Fong et al. 2014), so in order to allow a good number of simulations, we took a value at the wide end of those predicted, and selected from the Singer et al. (2014) simulations all those with a binary inclination⁵ $i \leq 30^\circ$, resulting in ~ 200 simulated objects each year (corresponding to $\sim 40\%$ of the mergers ‘detected’ in the Singer et al. 2014 simulations). Singer et al. (2014) provided two probability maps – all-sky maps where each pixel’s value is the probability that the GW event occurred in that pixel – one map was derived rapidly using an algorithm called BAYESTAR, the second created using a full Markov Chain Monte Carlo (MCMC) analysis, which takes much longer to run (typically ~ 109 hr according to Berry et al. 2015). We used the BAYESTAR maps, since these are available for all of the triggers on the LIGO website (the MCMC map is not), and because, due to their rapid creation and their similarity to the full MCMC results (for 2015, at least) they are likely to be the maps that will be used for real XRT follow-up of a GW trigger.

As noted above, these simulations were distributed homogeneously in space, whereas NS-NS mergers are expected to occur in or near to galaxies, so we needed to modify the spatial distribution of the simulated GW events to reflect this expectation. This can be done relatively simply, because the shape of the GW error region is determined not by the celestial location of the merger, but by the geocentric coordinates. This means that we can shift the simulated mergers and probability map in RA without invalidating them, provided we also adjust the trigger time such that the GRB

⁴ <http://www.ligo.org/scientists/first2years/>

⁵ While binary inclination angle is normally given in the range 0° – 90° , the GW simulations differentiate between clockwise and anticlockwise rotations, allowing i to be in the range 0–180; therefore we formally selected objects with $i \leq 30^\circ$ and $i \geq 150^\circ$.

is at the same geocentric position as in the original simulations.

Therefore, for each GW simulation we determined the completeness of the GWGC at the distance of the GRB (Table 1). For objects less than 100 Mpc away (i.e. the distance range covered by the GWGC), a random number was generated to determine whether this object should lie in a GWGC galaxy⁶. If it should, a galaxy was selected at random⁷ from those within the GWGC which had a distance consistent with that of the simulated merger, and a declination within 3° of the original LIGO simulation⁸. A position was randomly selected within this galaxy, with uniform probability through the galaxy, and then a kick of random magnitude (up to 100 kpc) and direction was applied to it. The GW probability map was then rotated on the celestial sphere such that the GRB lay at this position. For mergers where the random number determined that it was not inside a GWGC galaxy, or mergers at a distance greater than 100 Mpc (i.e. not covered by the catalogue) no shift was applied.

For each merger, regardless of whether we repositioned it, the day of the trigger was selected at random. The time of day at which the merger would lie at the geocentric location used for the GW simulations on this day was determined: this was set to be the GRB trigger time. For the 2015 simulations, the times were all in a 90 day window starting on 2015 September 1 (i.e. approximately the time expected to be covered by the science run); for 2016 we used a 180 day window starting in mid June. The only impact this has on the simulations is to set the positions of the Sun and Moon, hence the regions of sky which *Swift* cannot observe.

As well as the GRB location, distance and error region just described, the following two parameters were also needed for each simulation:

Time delay, τ_d – the time interval in hours between the GW trigger, and the commencement of *Swift* observations. Since the initial GW probability map will be produced within minutes of the trigger (Singer et al. 2014)⁹, we drew τ_d at random from the distribution of delay times found in the *Swift* follow-up of IceCube neutrino triggers (Evans et al. 2015), which is a reasonably analogous ToO programme. This is well modelled as a Lorentz distribution:

$$P(\tau_d) = \frac{N_l}{1 + \left(2 \left[\frac{\tau_d - C_l}{W_l} \right] \right)^2} \quad (1)$$

where $P(\tau_d)$ is the probability of the delay being τ_d , $N_l = 1103$, $C_l = -1.95$ hr and $W_l = -8.97 \times 10^{-2}$ hr.

X-ray afterglow template. For each simulation we selected at random one of the sGRBs listed in

Rowlinson et al. (2013)¹⁰, for which a valid light curve fit exists in the live XRT GRB catalogue¹¹ (Evans et al. 2009). We then took the automatic multiply-broken power-law fit to XRT light curve from this catalogue, and ‘shifted’ it to the redshift of the GW simulation by applying luminosity distance and time dilation corrections. For those sGRBs where the redshift was not known, we assumed the mean value of 0.72 (Rowlinson et al. 2013)¹². We did not apply a k-correction, to keep the simulations as simple as possible, having first verified that this made little difference: even in the most extreme case (taking a short GRB from $z = 2.6$ to simulate a NS-NS merger at 9 Mpc) the k-correction would make $\lesssim 10\%$ difference to the light curve normalisation. We can only use as templates those sGRBs for which we have a valid light curve fit, which introduces a bias: we have light curve fits for 29 of the sGRBs listed in Rowlinson et al. (2013) (of the remaining 14, 6 were not detected by XRT, and for the others we have only a single light curve bin, or a bin and an upper limit, so no fit is available). Thus, we are really simulating the brightest (in terms of flux, not luminosity) 67% of sGRBs observed by XRT. As will be seen in Section 7, this bias is not important when compared to other considerations.

In order to marginalise better over these different parameters, we performed this process (from deciding whether to shift the GW simulation onwards) ten times for each GW simulation, giving 2,350 simulations for 2015, and 1,930 for 2016.

3.1 Defining the XRT follow-up

At the present time it is not known how many fields it is practical to observe with *Swift* immediately after a GW trigger¹³; nor do we know how many we would choose to observe, since a point of diminishing returns is likely to exist (i.e. where observing extra fields barely increases the probability of detecting the GRB). The number of fields observed is therefore also a parameter we wish to explore. Initially, we created up to 2,400 XRT fields per GW simulation – more than we expect to observe in reality – by splitting the sky into a pattern of overlapping XRT fields, integrating the probability in the GW map within each field, and selected those with the highest probability (up to 2,400 fields, or where the probability of the event lying in a field fell below 10^{-6}). We did this in two ways: (1) integrating the probability from the original GW probability map, and (2) by integrating the probability from the GW map convolved with the GWGC mask (Section 2.2.1).

In order to realistically simulate XRT observations, the following information was produced for each field, in addition to the probability of it containing the GRB.

- (i) **The mean X-ray background level.** This was

⁶ i.e. the random number, R , had a value in the range $0 \leq R < 1$. If the GWGC was, e.g. 70% complete at the merger distance, then the merger was considered to be in a GWGC galaxy if $R \leq 0.7$.

⁷ A better approach would be to weight the galaxies by luminosity, however since we cannot move the Singer et al. (2014) simulations in RA this is not possible.

⁸ It is not practical to require the shift to be purely in RA; however a 3° declination shift is so small that the GW probability maps are not invalidated by this shift.

⁹ There may be an initial process of human screening before the map is distributed, but this is still being debated, so we have ignored it.

¹⁰ i.e. with a BAT $T_{90} \leq 2$ s, and to which *Swift* slewed promptly upon detection.

¹¹ http://www.swift.ac.uk/xrt_live_cat

¹² D’Avanzo et al. (2014) used a slightly different criteria for selecting sGRBs, and found a mean redshift of 0.85.

¹³ Investigative work is under way.

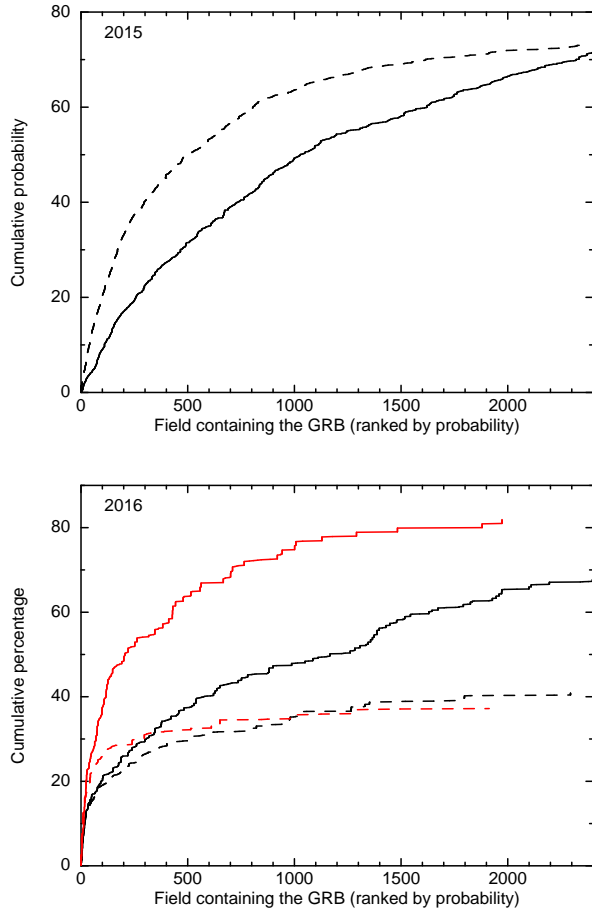


Figure 1. The impact of targeting galaxies. When 2,400 XRT fields are created to cover the most probable region of the ALIGO error region, the solid line shows the cumulative distribution of which field (ordered by probability) the GRB actually lies in. The dashed line shows the same, if the ALIGO error region is first convolved with the GWGC (Section 2.2.1). *Top:* The 2015 ALIGO configuration (based on the BAYESTAR probability map). Using the GWGC fewer fields are needed to reach a given probability of observing the GRB. *Bottom:* The 2016 ALIGO-AVirgo configuration: the BAYESTAR-based results are in black, those derived from the full MCMC error region are in red. Using the GWGC reduces the number of GRBs observed, because most of them occur beyond the 100 Mpc limit of GWGC catalogue.

drawn at random from the distribution of such levels seen in the 1SXPS catalogue¹⁴ (Evans et al. 2014).

(ii) **Details of any catalogued X-ray sources in the field.** These were taken from the RASS. The expected 0.3–10 keV XRT count rate was derived from the *Rosat* count rate using PIMMS and assuming a typical AGN spectrum: an absorbed power-law with $N_{\text{H}} = 3 \times 10^{20} \text{ cm}^{-2}$, $\Gamma = 1.7$.)

(iii) **The 3- σ RASS upper limit in the field.** This was derived using the RASS images, background maps and exposure maps¹⁵, and the Bayesian method of

Kraft, Burrows & Nousek (1991). This was converted to an XRT count-rate using PIMMS as above.

(iv) **Details of uncatalogued X-ray sources coincidentally in the field.** We derived these using the log N -log S distribution of Mateos et al. (2008), which gives the sky density of extra-galactic X-ray sources as a function of flux. From this we determined the expected number of sources unrelated to the GW trigger (N_s) in the field of view, with a flux of at least $10^{-13} \text{ erg cm}^{-2} \text{ s}^{-1}$ (this limit was chosen as it is well below the detection limit of *Swift*-XRT in the exposure durations we are going to explore). Then, drew the number of sources ($N_{s,r}$) in this simulated field at random from a Poisson distribution with a mean of N_s . If this number was greater than the number of sources already identified in step (ii) then we assigned extra sources to the field, until it contained ($N_{s,r}$) sources. The fluxes of these sources were drawn at random from the Mateos et al. (2008) log N -log S distribution, up to a maximum flux equivalent to the RASS upper limit for the field. We converted from flux to an XRT count-rate using the AGN spectrum defined in step (ii).

(v) **The visibility windows of the field for *Swift*-XRT,** for an interval of 15 days starting at the trigger.

Having thus generated 2,400 fields, the most probable N can be selected as inputs to our simulated observations, where N is one of the parameters the simulations are designed to explore.

3.2 Simulating the observations

Having defined the fields for XRT follow-up, we simulated the actual XRT observations for different observing strategies, to evaluate the impact of those strategies on how many sGRBs which trigger ALIGO/AVirgo we can identify with *Swift*-XRT. The strategies were based on two parameters: the number of XRT fields (N), and the exposure per observation (e). We explored values of $N = 50, 100, 200, 600, 1200$ and 1800, and $e = 10, 50, 100$ and 500 s. This was done both for the fields based on the raw GW probability map and those based on the convolution with the GWGC catalogue.

We simulated 15 days of observations, recording after each field was observed whether the GRB had been identified, and also how many uncatalogued sources which were not the GRB had been identified. Full details of how the fields to be observed were selected are given in Appendix A.

4 RESULT 1: SHOULD WE TARGET GALAXIES?

4.1 2015

To investigate the effect of convolving the GW error region with the GWGC (Section 2.2.1), we recorded which field (ordered by decreasing probability) the GRB actually lay in. Not all GRBs lay within the 2,400 most probable fields, regardless of whether galaxy targeting was employed. For the 2015 ALIGO configuration, the number of bursts which did lie in these regions was barely affected by use of the GWGC: 1,291 (/2,350) GRBs lay inside the most-probable 2,400 fields whether or not the GWGC was used; 425 GRB only lay in these fields if the GWGC was used, and 394 were only present if the GWGC was not used. However, use of

¹⁴ We used the 0.3–10 keV background count-rate (‘FIELDDBG0’) from all 1SXPS fields with a ‘FIELDFLAG’ of zero (i.e. they contained no artefacts or extended sources).

¹⁵ Obtained from <ftp://ftp.xray.mpe.mpg.de/ftp/rosat/archive>

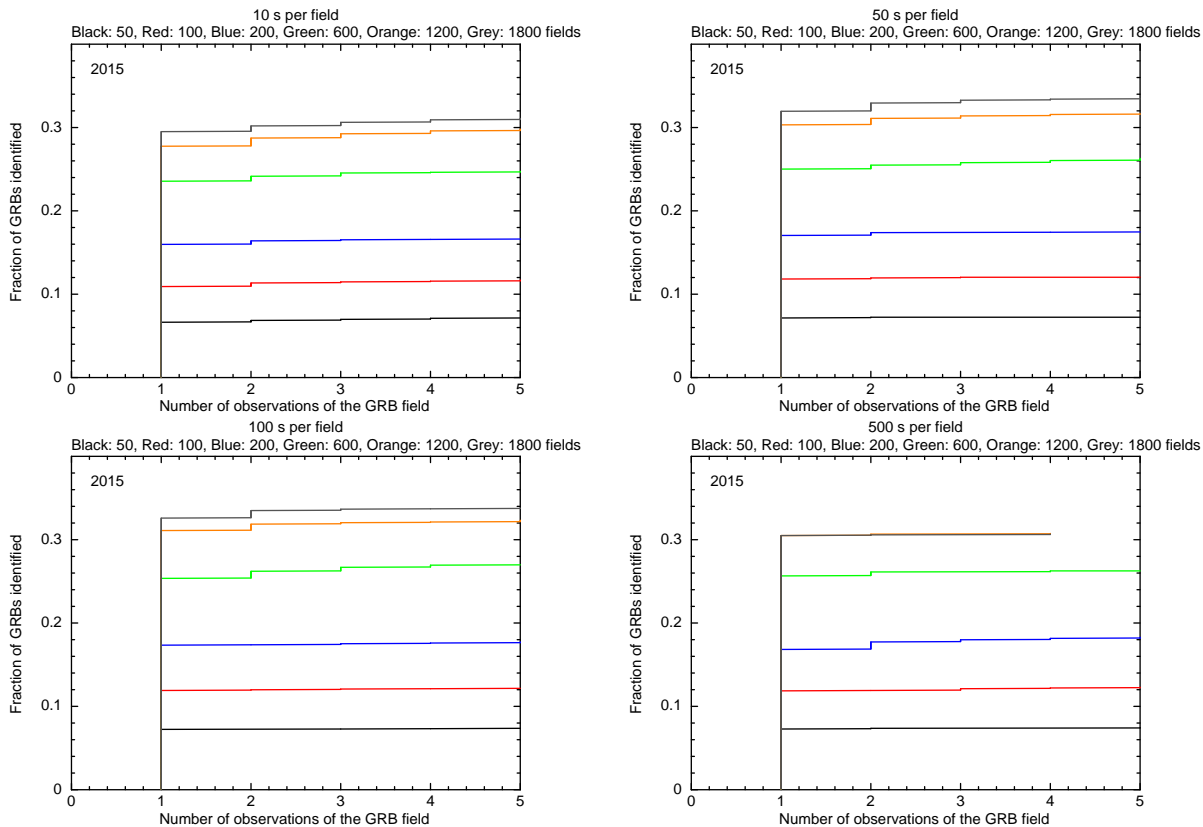


Figure 3. The fraction of GRBs identified as a function of how many observations of all fields have been performed. This is for the 2015 configuration simulations, with galaxy targeting. The 4 panels are for the 4 values of e (exposure per observation) we simulated, and the different colours refer to different values of N (the number of fields).

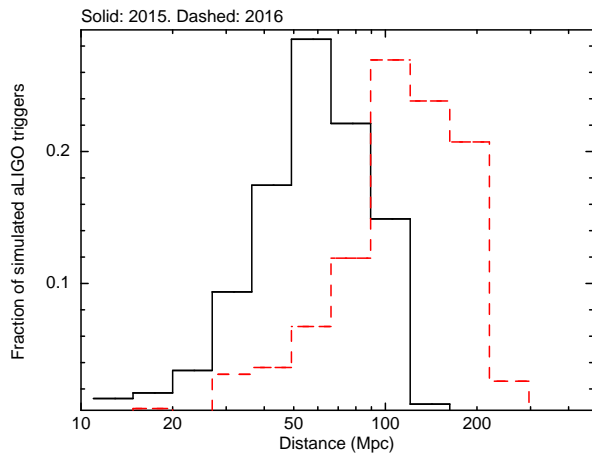


Figure 2. The distribution of the simulated NS-NS mergers detected by the simulated 2015 ALIGO configuration (solid black) and 2016 ALIGO+AVirgo configuration (dashed red). Both plots are normalised to 1.

the GWGC enables the GRB to be observed quicker. Fig. 1 shows the cumulative distribution of which field contained the GRB, for both approaches. Convolution the ALIGO error with the GWGC means that we need observe far fewer fields to image the GRB. For example, to contain 50% of the ALIGO triggers if we use GWGC convolution, we need ob-

serve ‘only’ 500 fields; without the convolution 1,030 fields are needed.

In summary: for 2015 it is best to target galaxies provided the GW events arise from NS-NS binaries. For NS-BH binaries, the horizon distance of aLIGO is greater, and the situation is more akin to the 2016 NS-NS case discussed below.

4.2 2016

For 2016 the situation is very different. Unlike 2015, most of the NS-NS mergers detected were more than 100 Mpc away (see Fig. 2) and so do not reside in GWGC galaxies. In consequence, targeting those galaxies reduces the number of NS-NS mergers that lie in XRT fields. Thus for the 2016 configuration, targeting GWGC galaxies is detrimental to our chances of detecting the X-ray counterpart to a GW trigger. Without galaxy targeting, the typical number of fields required to image the merger location in 2016 is similar to that in 2015. That is, the 2016 configuration increases the horizon distance without reducing the size of the error region. However, this is a software issue. Singer et al. (2014) show (their fig. 3) that for the 2016 configuration the fast BAYESTAR algorithm which is used to construct the GW error region does not perform particularly well, and results in a larger-than-necessary error region. The full MCMC approach typically gives much smaller error regions; however

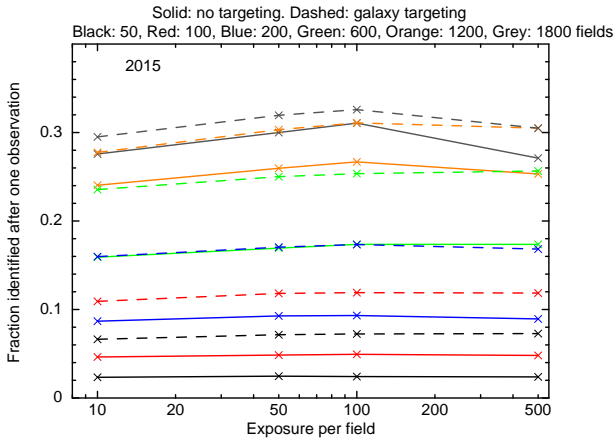


Figure 4. The fraction of GRBs identified in the 2015 simulations, after a single observation of all N fields, as a function of the exposure per observation. The solid lines show the result when the N fields are based on the raw ALIGO probability map, and the dashed lines for if the map is first convolved with the GWGC.

it also takes much longer to run, (‘hours to days’ according to Singer et al. 2014), which makes waiting for it impractical. Singer et al. (2014) were optimistic that, by 2016, the time delay may have been dramatically reduced. Indeed, the latest news (Singer, private communication) is that the MCMC process has been made faster, and BAYESTAR has been improved and now performs as well as the full MCMC for the 2016 configuration. Therefore, the full MCMC probability maps from Singer et al. (2014) are more representative of what the rapidly available BAYESTAR maps will actually be like in 2016, so we repeated our simulations for 2016, this time using the MCMC probability map instead of BAYESTAR. Unfortunately, only 100 of the 193 on-axis mergers for 2016 in Singer et al. (2014) had MCMC probability maps, resulting in lower statistics. However, Fig. 1 shows that, with MCMC, the situation is dramatically improved. It is of course still true that use of the GWGC is detrimental, since most mergers in 2016 lie beyond that catalogue’s distance horizon, however even without galaxy targeting, the smaller error regions available in 2016 actually mean that it takes fewer fields on average to observe the location of the GRB than with galaxy targeting in 2015. As noted earlier (Section 2.2.1), other catalogues such as 2MPZ may be appropriate for use in 2016.

In summary: for 2016 the GW regions should not be convolved with the GWGC. Other galaxy catalogues may be appropriate, provided their completeness out to 200–300 Mpc can be derived and shown to be substantial.

5 RESULT 2: OPTIMAL OBSERVING STRATEGY

5.1 2015

The previous section demonstrated that, for the 2015 configuration, it is preferable to target galaxies in the ALIGO error regions. In Fig. 3 we show the fraction of the galaxy-targeting simulations for which the GRB was identified, as a function of how many observations of the N fields were conducted. This is shown for all values of N (different coloured

lines) and e (different panels) used in our simulations. Recall that we only simulated on-axis GRBs, therefore this is the fraction of such GRBs, not the fraction of merger events in total. For all of the configurations we tested, almost every GRB identifiable is identified in the first observation of its field: repeat observations have little value, as far as identifying the bright X-ray object is concerned. The exposure dependence is illustrated more clearly in Fig. 4, where we show the fraction of GRBs identified after a single observation of all N fields, as a function of the exposure time per observation. Little exposure dependence is seen, except for the combination of large values of e and N , where the fraction identified drops slightly. This is because, in such cases it takes so long to reach the field containing the GRB that fades below the RASS limit before it is observed. Fig. 4 also includes the simulations with and without galaxy targeting, clearly demonstrating the value of galaxy targeting in 2015.

In a very small number of the simulations ($\sim 0.05\%$) the GRB was detected, but was not bright enough to be identified. In this case, a second observation could be performed to identify fading behaviour in the source. However, this is a very inefficient approach. As Fig. 5 shows, most strategies will result in the detection of new, uncatalogued sources which are not the GRB, all of which would have to be followed up; and as already noted, the number of cases where the GRB is among these sources is extremely small.

5.1.1 False positives

We noted earlier (Section 2.1) that the expected rate of X-ray transient sources is 1 per 1.64 Ms of exposure time. So for the case of 600 fields, observed for 50 s each, there is only a 2% chance of serendipitously observing a X-ray transient unrelated to the GW trigger. There is, however, an additional source of potential contamination: due to Poisson noise, an uncatalogued source with a flux below the RASS limit will sometimes be measured to have a flux more than $1\text{-}\sigma$ above this limit, thus meeting one of our criteria to be identified as the likely GRB afterglow. Our simulations included Poisson noise, and we recorded how many of the unrelated sources detected would be thus classified as a possible afterglow. Fig. 6 shows the fraction of simulations in which this happened for at least one unrelated source. This increases sharply for exposures longer than 50 s. This means that we cannot interpret the discovery of a bright ($>$ RASS limit), uncatalogued source to be an unambiguous detection of the sGRB: it could simply be a fainter source subject to Poisson errors. Also, there could be multiple ‘bright’ sources detected in the follow-up of a single GW trigger. Therefore, it will be necessary to re-observe any such sources for ~ 1 ks each to confirm which (if any) of them was a transient event. The maximum number of such false positives detected in any of our simulations is 19, so this confirmation observation requires only a small investment of exposure time, compared to that used to detect the sources.

5.2 2016

We performed two sets of simulations for 2016, one based on the BAYESTAR error maps and one based on the full MCMC maps. Since Fig. 1 showed that targeting GWGC galaxies was detrimental in 2016, we only simulated observations

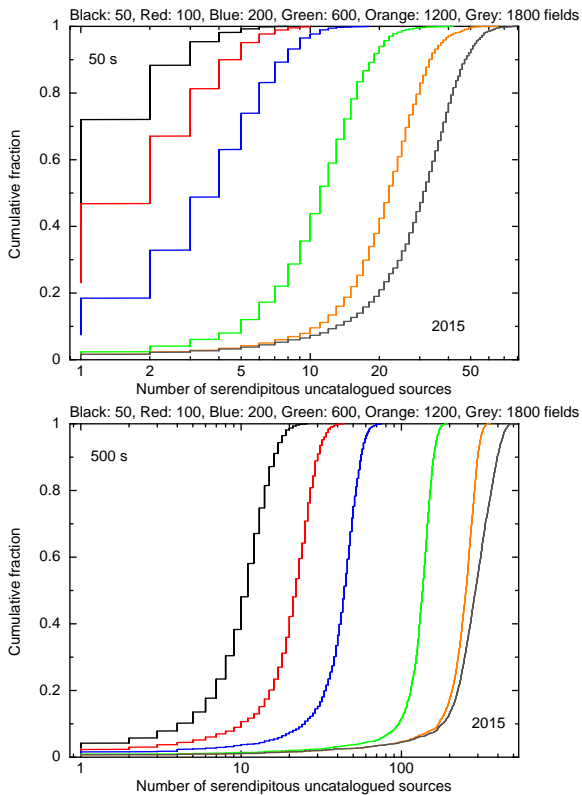


Figure 5. The cumulative distribution of the number of uncatalogued sources unrelated to the GW trigger detected in the 2015 simulations (with galaxy targeting), assuming observations of 50 s (top panel) or 500 s (bottom). If no bright source is detected in the observations, all of these uncatalogued sources would have to be reobserved to search for signs of fading.

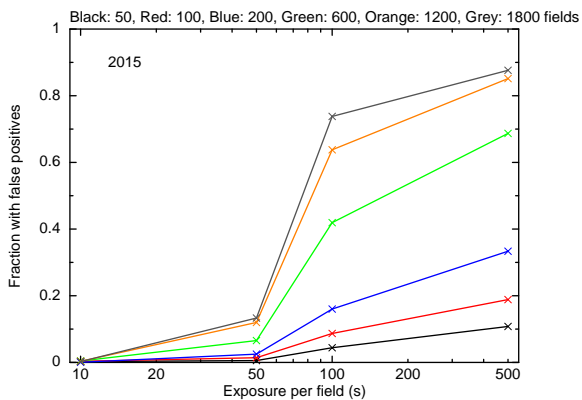


Figure 6. The fraction of simulations in which a source unrelated to the GW trigger was classified as a potential afterglow, because its measured flux was above the RASS limit due to Poisson noise. The data shown here are for the 2015 simulations, with galaxy targeting.

based on the raw GW error maps. As with the 2015 simulations almost all identifiable GRBs were identified in a single observation. Fig. 7 shows the fraction of GRBs detected as a function of exposure time, for the different simulations, an analogue of Fig. 4. Using the BAYESTAR maps we identified a lower fraction of GRBs than in the 2015 simulations, al-

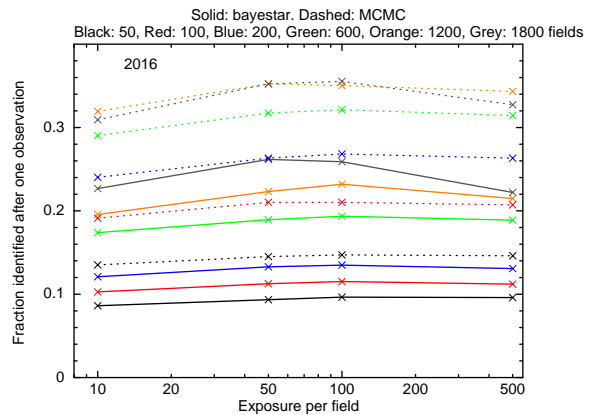


Figure 7. The fraction of GRBs identified in the 2016 simulations, after a single observation of all N fields, as a function of the exposure per observation. The solid lines show the result if the BAYESTAR error map is used, and the dashed lines are for the full MCMC error map.

though for the $N \leq 200$ simulations, the difference is less obvious: the fraction identified in 2016 is comparable to the 2015 follow-up with no galaxy targeting. In contrast, using the full MCMC-based error map in 2016 we identified the GRB in a larger fraction of simulations than in 2015.

One curious feature of Fig. 7 is that, for the $N = 1,800$ simulations based on the full exposure map, fewer GRBs were identified than the $N = 1,200$ simulations at $e = 500$ s. This is an artefact of the way the simulations decide in which order to observe the XRT fields (Appendix A), which means that while the fields in the $N = 1,200$ simulation are the most probable 1,200 fields in the $N = 1,800$ simulation, they are not necessarily the first 1,200 to be observed in the latter simulations. This, combined with the spatial distribution of probability in the 2016 MCMC error maps, which tends to contain distinct ‘clumps’, means that on average the field which actually contained the GRB was observed later in the $N = 1,800$ simulations than in the $N = 1,200$ case. As a result, the GRB was more likely to have faded to below the detection threshold or RASS limit.

6 IF *FERMI* TRIGGERS AS WELL

If *Swift*-BAT and ALIGO/AVirgo trigger on the same event, the discussion in this paper is moot: the BAT error region fits comfortably in the XRT (and UVOT) field of view, and the satellite will perform the standard automatic follow-up process which has resulted in the rapid detection of the X-ray afterglow of almost all sGRBs detected by *Swift*-BAT to date. However, as noted earlier, this is unlikely. A more probable scenario for the simultaneous GW and EM detection of the same event is for *Fermi* to trigger on the GRB. *Fermi* contains two instruments: the Gamma-ray Burst Monitor (GBM; Meegan et al. 2009) and Large Area Telescope (LAT; Atwood et al. 2009). GBM is sensitive to triggers over the entire sky which is unocculted by the Earth, although has poor positional accuracy, with typical uncertainties of many degrees. LAT has a smaller field of view (2.4 sr), and if GBM detects a bright GRB *Fermi* with a sufficiently high peak flux, *Fermi* automatically slews to

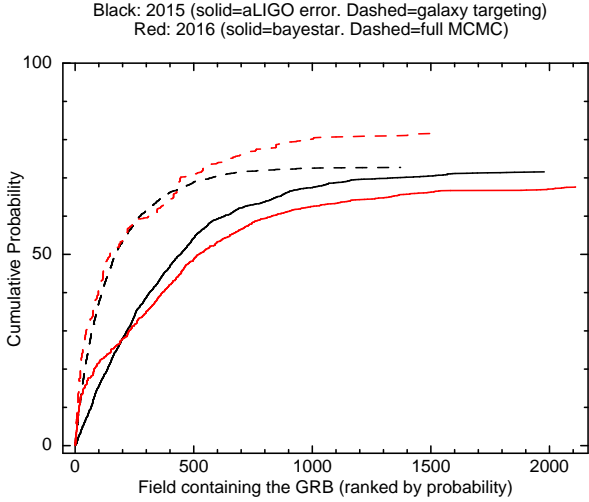


Figure 8. As Fig. 1 but showing the effect of using information from a *Fermi*-GBM trigger simultaneous with the GW trigger. The black lines are for the 2015 ALIGO-detected mergers, with the dashed and solid lines showing respectively whether the GWGC is or is not used. The red lines show the 2016 ALIGO/AVirgo objects, with the solid line showing the BAYESTAR probability maps and the dashed line the full MCMC map.

move the GRB into the LAT field of view (Ackermann et al. 2013; von Kienlin et al. 2014). LAT positions can be much better than those from GBM, down to $\sim 0.1^\circ$. While it is beyond the scope of this work to simulate the probabilities of these instruments triggering on GW-detected sGRBs, we consider how such triggers will influence *Swift* observations. Note that, due to their proximity, we would expect such sGRBs to be bright enough to trigger *Fermi* (or indeed BAT or the Interplanetary Network [IPN]) unless they are ~ 100 times fainter than the typical *Swift*-detected sGRBs (see Section 7).

6.1 If LAT triggers

While the LAT error region is highly variable, at the lower end they are small enough to fit inside a single XRT field of view. For less-well constrained positions, *Swift* has often observed the LAT error region in a small number of tiles (typically 4, sometimes 7; e.g. Evans 2013). This allows us to rapidly cover the entire error region, and build up long exposures of multiple kiloseconds per tile in much less time that it takes to observe each field once if we have only a GW trigger. These longer exposures allow easy identification not just of a bright source, but also of a faint, but clearly fading object. Due to the small area covered, the possible presence of unrelated sources is not a significant issue, since the burden of following multiple sources to confirm their behaviour is much reduced when those sources are close together. A drawback to LAT triggers is that nearly all of them are found in ground processing, which means that are not detected until many hours after the event. However, a nearby burst will likely also be bright, increasing the likelihood of an onboard LAT trigger. Further, even if *Swift* has already started tiling the GW error region, should a LAT error re-

gion become available, we could immediately terminate the ongoing observations and point *Swift* at the LAT region.

6.2 If GBM triggers

Even if LAT does not detect the GRB, a GBM detection simultaneous with an ALIGO/AVirgo trigger has the potential to significantly reduce the sky area we need to search. The median $1\text{-}\sigma$ statistical error radius for a GBM-detected sGRB¹⁶ is 7° . A systematic error is also present (Connaughton et al. 2015), which we simplistically treat as a Gaussian with $\sigma=3.7^\circ$, giving an overall error median error of 8° . For each simulated GW event in our samples, we selected at random the location of the centre of the GBM error region, assuming a circular region, with a Gaussian radius, with $\sigma_{\text{tot}} = 8^\circ$, and then created the list of XRT fields to observe as in Section 3, but also only accepting fields that lay within $3\text{-}\sigma_{\text{tot}}$ of the simulated GBM position. We then determined how many fields we would have to observe (to a maximum of 2,400) in order to observe the GRB location. The result is shown in Fig. 8, which can be compared with Fig. 1. This shows, not surprisingly, that if a GBM localisation is available, it can reduce the number of XRT fields we need to observe significantly, e.g. in 2015, with galaxy targeting, the number of XRT fields needed to observe 50% of the GRBs is just 190 (compared to 500 without GBM: see Section 3.2).

7 ARE DETECTABLE, NEARBY SGRBS LIKELY?

So far we have focussed on how best to search for an XRT counterpart to a GW trigger, but another important consideration is whether a GW trigger from a nearby, on-axis sGRB is likely. Various works have attempted to calculate the rate of nearby sGRBs, either from the theoretically expected merger rate (e.g. Abadie et al. 2010) or the rate of observed sGRBs (e.g. Coward et al. 2012). As noted earlier, these estimates have large uncertainties, for example, Coward et al. (2012) give an sGRB rate density of $\sim 8 - 1100 \text{ Gpc}^{-3} \text{ yr}^{-1}$. Metzger & Berger (2012) fitted the observed redshift distribution of *Swift*-detected sGRBs with known redshift, divided this by the fraction of sGRBs with known redshifts, and from that inferred that “a few *Fermi* bursts over the past few years probably occurred within the ALIGO/Virgo volume.” However these approaches do not consider one important observational constraint: unless the nearby sGRBs are systematically less luminous than the ones for which we have redshifts, they should appear much brighter than those – orders of magnitude brighter. Is there evidence for any such bright objects among the sGRBs detected to date?

To investigate this we want to compare the expected brightness of an sGRB inside the ALIGO/Virgo horizon with the distribution of observed sGRB brightnesses. We

¹⁶ Taken from the *Fermi* GRB catalogue, Gruber et al. (2014); von Kienlin et al. (2014), <http://heasarc.gsfc.nasa.gov/W3Browse/fermi/fermigbrst.html>, selecting objects with $T_{90} < 2 \text{ s}$ and $\text{FLUX_BATSE_64} > 2.37 \text{ s}^{-1}$, following Wanderman & Piran (2015).

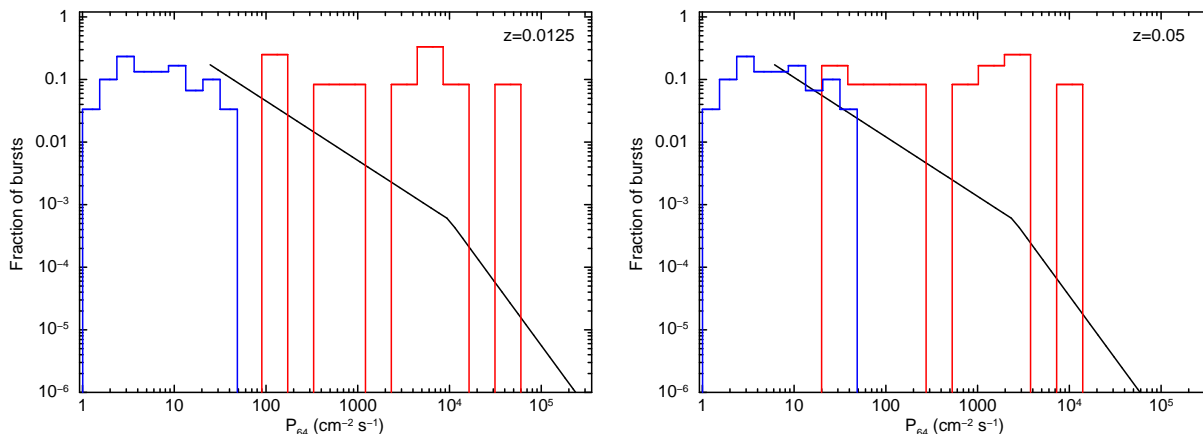


Figure 9. A comparison of the observed brightness of the *Swift*-sGRBs without redshift, to what would be expected from an sGRB within the GW horizon distance. P_{64} is the peak 64-ms photon flux. The blue histogram shows the distribution of P_{64} for the *Swift* short GRBs without redshift. The red histogram shows the distribution of short GRBs with redshift measurements, with the peak flux corrected to a distance of 100 (left panel) or 200 (right panel) Mpc. The resultant peak fluxes are orders of magnitude larger than anything *Swift* has observed to date. The solid black line shows the theoretical sGRB luminosity function of Wanderman & Piran (2015), converted to P_{64} at the two distances.

define the brightness as the 64-ms peak photon flux (P_{64}) from the prompt emission, following Wanderman & Piran (2015). For the *Swift*-detected sGRBs with known redshift listed in Wanderman & Piran (2015), we derived the 15–150 keV P_{64} values that would have been measured had the GRB been at $z = 0.025$ (~ 100 Mpc) and $z = 0.05$ (~ 200 Mpc); these are shown as red histograms in Fig. 9. This sample is likely biased towards intrinsically brighter objects (i.e. objects which are easier to detect), so we have also converted the theoretical luminosity function of short GRBs from Wanderman & Piran (2015) into the distribution of 15–150 keV P_{64} at these two redshifts; this is shown as the black line in Fig. 9. For comparison, we also show the distribution of the observed 15–150 keV P_{64} values for the *Swift*-BAT detected sGRBs without a known redshift (blue histograms). The P_{64} distribution of the *Swift* sGRBs with no redshift is clearly not consistent with them being identical to the known-redshift sample but lying at low redshift: in this case the blue histograms would appear similar to (or at least share significant overlap with) the red ones. It is possible that a small number of the no-redshift sample were at ~ 200 Mpc, however they must have been of lower intrinsic luminosity than the with-redshift sample, since they just barely overlap with what the latter sample would have looked like at 200 Mpc. We certainly cannot rule out that some of the no-redshift sample lay at 100–200 Mpc and came from the faintest end of the Wanderman & Piran (2015) luminosity function, although this faint end is not well constrained. There are, however, two objections to this premise. First, the *observed* P_{64} distributions of the with- and without-redshift *Swift* sGRB samples are very similar (Fig. 10): a Kolmogorov-Smirnov test gives the probability that the two samples are drawn from the same distribution as 0.43; so if the no-redshift sample does indeed contain bursts that are of lower luminosity than the with-redshift sample, the redshift distributions of the two samples have fortuitously been tuned correctly to give apparently identical P_{64} distributions, which seems a little far-fetched. Sec-

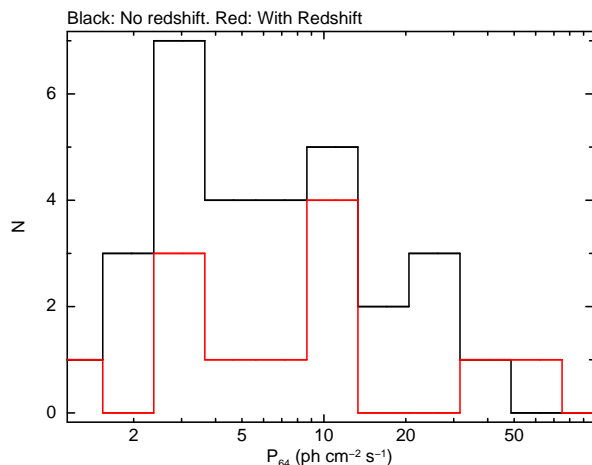


Figure 10. The distribution of observed peak 64-ms photon flux from the *Swift* GRBs with redshift (red) and without (black). The K-S test gives a 0.43 probability that the two samples come from the same parent distribution.

ondly, if any of the no-redshift sample really were within 200 Mpc, we would expect the host galaxy to have been found in optical follow-up, and hence the GRB to have a redshift. Tunnicliffe et al. (2014) explored this question and found tentative evidence that one or two ‘hostless’ sGRBs could have arisen from stars kicked out of nearby (< 200 Mpc) galaxies but that these would have surprisingly low jet energies. For example, they found a galaxy at a distance of 80 Mpc, which *could* be the host of GRB 111020A, but this would require the isotropic equivalent for that GRB to be just 10^{46} erg, several orders of magnitude lower than typical sGRBs. These considerations suggest that no compelling evidence exists for a BAT-detected sGRB within 200 Mpc.

Swift-BAT detects fewer sGRBs than GBM does or BATSE did, so we have repeated the above test, for the BATSE and GBM bursts. The results are shown in Fig. 11.

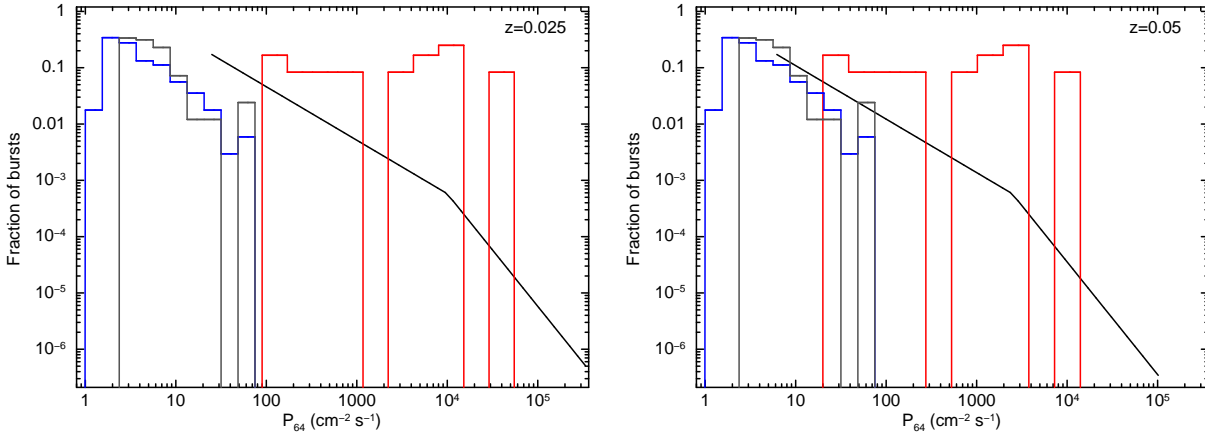


Figure 11. As Fig. 9 but for the 50–300 keV band. The blue and grey histograms show the distribution of observed peak 64-ms photon flux for the BATSE and GBM sGRBs respectively – these have no measured redshift.

For these, we derived P_{64} in the 50–350 keV band used by those instruments. We again plotted the expected P_{64} values for the with-redshift *Swift* sGRBs (corrected to the 50–350 keV band), had they been at 100 or 200 Mpc (red histograms). The BATSE and GBM observed P_{64} distributions are shown in the blue and grey histograms respectively. As with the *Swift* data, we cannot rule out the possibility that a few of the sGRBs detected by BATSE or GBM could have been within 100–200 Mpc from Earth, however, again, these must have been significantly fainter (typically at least an order of magnitude) than the *Swift*-detected GRBs with redshift. A substantial fraction of the observed GBM and BATSE bursts are consistent with being at 200 Mpc, provided they come from the low-luminosity end of the Wanderman & Piran (2015) luminosity function. However, this cannot be systematically the case, since the GBM and BATSE samples must contain the more luminous GRBs that *Swift* has detected as well.

Two historic events warrant explicit mention: GRBs 051103 and 070201 were both very bright events, localised by the IPN, and with large error regions that partially intersected M81 and M31 respectively. However, LIGO observations showed that GRB 070201 could not have been a NS-NS or NS-BH merger in M31 (Abbott et al. 2008), suggesting instead that it was a giant flare from a soft gamma repeater (SGR), or a more distant sGRB coincidentally close in projection to M31. The case for GRB 051103 is less clear, and an SGR origin of this event cannot be ruled out. If it were a sGRB in M81 then it had a very low energy release (isotropic equivalent of $\sim 10^{46}$ erg) and an extremely faint afterglow (Hurley et al. 2010).

These considerations mean that we cannot conclusively rule out that some of the observed GRBs without redshifts could have been nearby – particularly those detected by BATSE, GBM or IPN, where the error regions are too large for host galaxy searches. However, we can state that, were this so, these nearby bursts were also underluminous compared to the with-redshift sample of *Swift* sGRBs. In more than 20 years of observations, no sGRB has been detected consistent with being less than 200 Mpc away and having a prompt luminosity typical of the *Swift* sample. This means that events such as those we have simulated in this work are

rare. So if ALIGO/Virgo does detect a binary NS merger, it is likely to be significantly fainter (1–2 orders of magnitude) than in our simulations, and therefore much harder to detect. More likely is that a NS-NS merger detected by ALIGO/AVirgo will be off-axis, that is, the jet will not be pointed towards Earth. For such objects no prompt gamma-ray emission is seen from Earth, so such objects are not in our observed GRB sample. Afterglow emission is still expected from some such objects however, and we now briefly consider how detectable such emission may be.

7.1 Off-axis GRBs

Although there are no X-ray observational constraints on the properties of GRBs viewed off-axis (by which we mean that the binary inclination i is larger than the jet opening angle, θ_j), there have been theoretical predictions (e.g. van Eerten & MacFadyen 2011; Ghirlanda et al. 2015). In order to give some indication of the potential observability of off-axis sGRB afterglows with *Swift* we have taken a highly simplified approach. First, we assumed that the time at which the afterglow becomes visible off-axis (t_{oa}), for a binary at inclination i radians, is the same as the time at which a jet-break would occur if the jet opening angle (θ_j) was i :

$$t_{\text{oa}} = \left(\frac{i}{0.13}\right)^{\frac{8}{3}} \left(\frac{E_{52}}{n_0}\right)^{\frac{1}{3}} \quad (2)$$

where E_{52} is the energy in the jet (E_{jet}) in units of 10^{52} erg, n_0 is the circumburst density in units of cm^{-3} , and t_{oa} is in the rest-frame of the GRB.

Rather than the generous value of 30° used earlier, we began by assuming a jet opening angle of 10° for all bursts (e.g. Duffell, Quataert & MacFadyen 2015). To simulate a GRB, we assigned it a distance D up to 200 Mpc (with probability $P(D) \propto D^2$) and a binary inclination i in the range 0 – 90° (with probability $P(i) \propto \sin i$). We selected an observed short GRB X-ray afterglow to use as a template, as in Section 3, but modified the light curve slightly to include a jet break (the jet break time calculated as in equation 2, but replacing i with $\theta_j = 10^\circ$), after which the light curve decayed with a power-law index of -2.5 . For

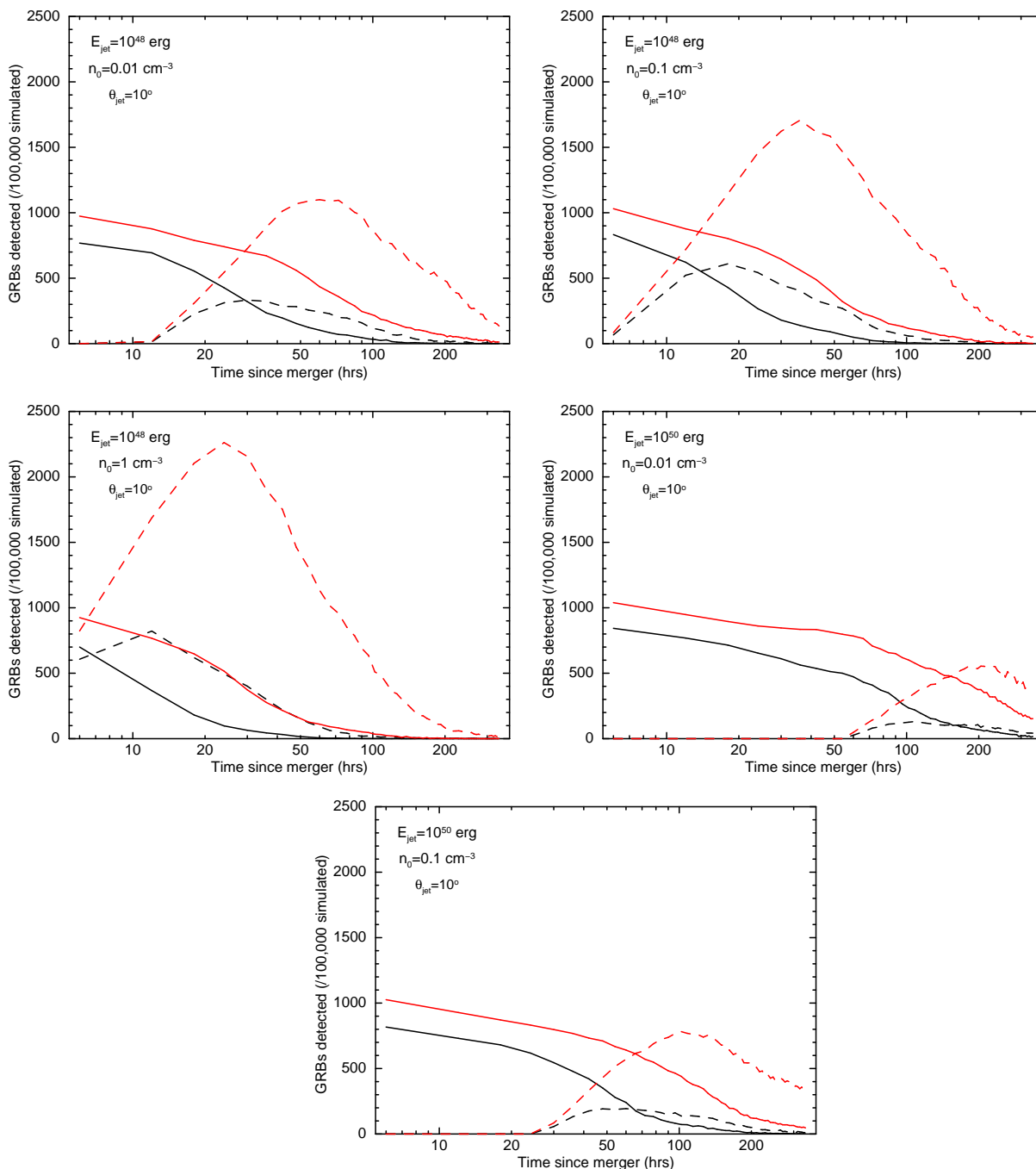


Figure 12. The number of bursts (out of 100,000 simulated) detectable in a 50 s (black) or 500 s (red) observation, as a function of how long after the merger the observation begins. The solid lines are bursts viewed ‘on-axis’, that is the 10° jet is oriented towards the observer. The dashed lines are the off-axis events. The different panels correspond to different values of jet energy (E_{jet}) and circumburst density (n_0). At early times the on-axis bursts dominate the visible population, despite comprising only 1.5% of all mergers. At late times, as the afterglow becomes visible off-axis, the off-axis population starts to dominate.

on-axis binaries ($i \leq 10^\circ$) the brightness of the GRB afterglow at a given time was taken from this light curve. For off-axis binaries, we assumed there was no X-ray emission before t_{oa} , after which the brightness followed the on-axis (post jet-break) light curve just defined. Comparison with the simulated light curves of van Eerten & MacFadyen

(2011)¹⁷ shows that this simplification is not unreasonable. We then calculated whether the GRB would be detected in observations of 50 s or 500 s, as a function of the time since the merger event (for these simple simulations we assumed

¹⁷ <http://cosmo.nyu.edu/afterglowlibrary/sgrb2011.html>

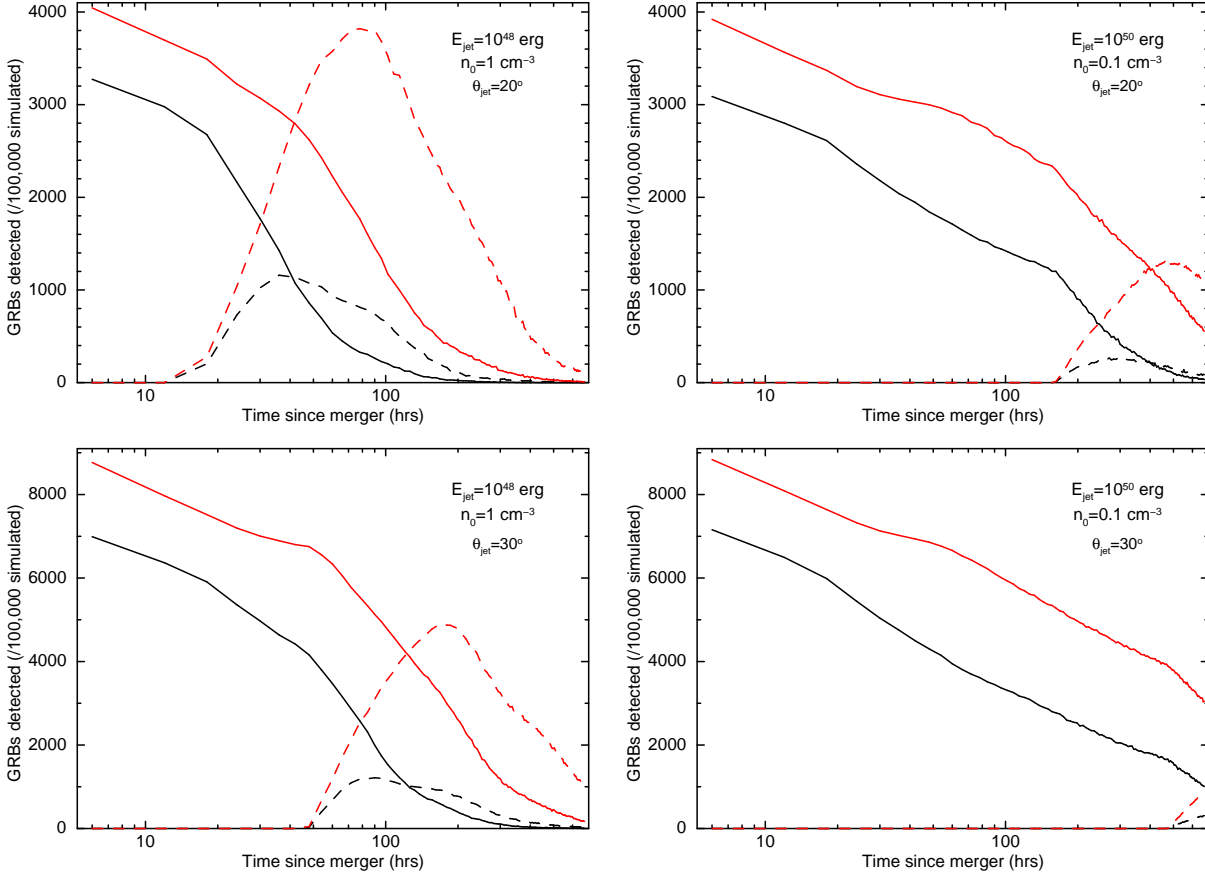


Figure 13. How many on/off-axis afterglows are detected as a function of time for jet angles of 20° (top panels) and 30° (bottom panels). Rather than reproducing all the panels of Fig. 12, we show only the densities which give the most off-axis bursts for each of the energies investigated. The solid lines are bursts viewed ‘on-axis’. the dashed lines are the off-axis events.

the XRT background level was always 10^{-6} ct s^{-1} pixel $^{-1}$, a typical value from 1SXPS; Evans et al. 2014).

We simulated 100,000 GRBs for each combination of $E_{52}=0.01$ and 0.0001 (following van Eerten & MacFadyen 2011), and n_0 of 0.01 , 0.1 and 1 cm^{-3} (e.g. Berger 2014). Note that, since t_{0a} and θ_j scale with E_{52}/n_0 , some of these combinations are degenerate.

In Fig. 12 we show the number of simulations in which the GRB was detectable in observations of 50 s or 500 s, as a function of the time at which the observation began. The on-axis and off-axis GRBs are differentiated. Although there are many more off-axis bursts (98.5% of those simulated), they are less detectable, since, by the time the emission becomes visible to the observer, it has faded significantly – Fig. 14 shows the cumulative distribution of binary inclinations for the GRBs detected and shows that this still corresponds to a fairly restrictive range of viewing angles. Fig. 12 shows that the detectability of the off-axis objects depends strongly on the jet energy and the circumburst density; in reality some (not currently constrained) distribution of these parameters is expected, which means that the ‘true’ shape of Fig. 12 for the short GRB sample is some form of weighted average of the panels shown.

This variation in detectability makes it difficult to define the optimal time to observe in X-rays in order to detect off-axis emission. For on-axis GRBs, it is clear that the

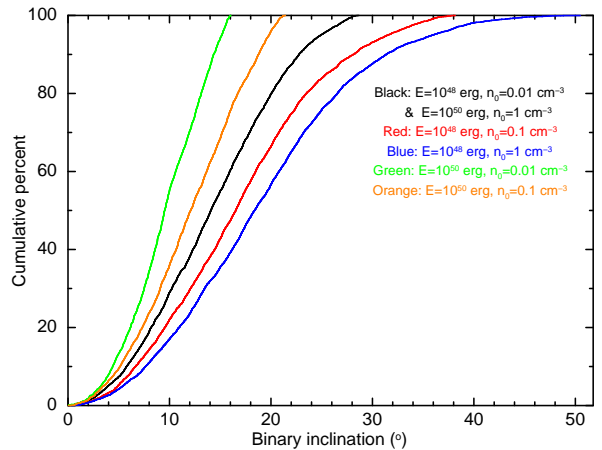


Figure 14. The cumulative distribution of binary inclinations for the mergers which were detected by our simulations, when the jet opening angle was 10° . The range of angles which result in detectable GRBs depends strongly on the jet energy and circumburst density.

earlier the observations, the more GRBs are detected. For off-axis objects, observing too early prevents detection (the afterglow emission is still beamed away from the observer),

as does observing too late (the emission is too faint), but the parameters of the window in which the afterglow can be detected vary according to the burst properties. Fig. 12 shows that by ~ 36 hours after the trigger, the number of off-axis bursts detectable exceeds the number of on-axis bursts for all $E_{52} = 0.0001$ simulations. For if $E_{52} = 0.01$ then on-axis bursts dominate until at least 72 hours post merger. A sensible *Swift* response to a GW trigger may therefore be to begin observations as soon as possible (in case the merger was on-axis), but after ~ 36 hours, if the afterglow has not been detected, the strategy should instead turn to looking for off-axis afterglows which are starting to emerge. In this case, rather than continuing the XRT observing program (which will be moving to lower-probability portions of the GW error region) it would be preferable to re-observe the high-probability fields already studied. This has an additional science bonus, in that if the GRB afterglow is detected in these second observations, but was not present in the first, it confirms that the merger was off-axis, and allows us to place constraints on $i - \theta_j$. One could envisage a third set of observations beginning at 72 hours after the trigger (i.e. where the off-axis start to dominate over the on-axis GRBs if $E_{52} = 0.01$). However at this time, the number of off-axis afterglows detectable if $E_{52} = 0.0001$ is still much higher than if $E_{52} = 0.01$, therefore unless there are compelling reasons to believe that the true sGRB population is dominated by the higher-energy objects, it is better to continue the observations than the return the the previously observed-fields.

We also see from Fig. 12 that the choice of exposure time is much more important for off-axis GRBs than for on-axis GRBs, with the number of off-axis GRBs detected a factor of 3–5 higher for 500 s exposures than for the 50 s exposures: for on-axis GRBs the difference is at most a factor of 1.5. Therefore, if this ‘double-headed’ approach were employed it would make sense to use shorter exposures in the first 36 hours, while searching for on-axis objects, and then switch to longer exposures when the search focus shifts to off-axis GRBs.

While the jet opening angle of 10° used above may be reasonably representative of typical jets (e.g. Duffell, Quataert & MacFadyen 2015), lower limits as large as 25° have been deduced for sGRBs (Grupe et al. 2006; Zhang et al. 2015). We repeated our simulations for jet opening angles of 20° and 30° , extending the runs to 28 days after the merger, to account for the later rise time of the off-axis jets. Fig. 13 shows the results for the values of E_{52}/n_0 which maximise the number of off-axis bursts detectable. Increasing the jet angle had two effects: some off-axis GRBs became on-axis GRBs, and the rise time of the off-axis GRBs moved to later times. The latter also means that the off-axis afterglows are fainter. These factors conspire to make the off-axis afterglow less significant as a proportion of afterglows detectable with XRT.

All of the considerations discussed in this section show that chasing off-axis afterglows with a narrow-field instrument such as *Swift*-XRT is extremely challenging. The number of such afterglows that can be detected, and the time at which they are detectable, are both highly variable, depending on the details of the jet and the medium in which burst occurs.

8 DISCUSSION AND CONCLUSIONS

We have performed simulations of *Swift*-XRT follow-up of GW triggers from the ALIGO/AVirgo observatories, according to their expected performance in the 2015 and 2016 science runs. In each case, we assumed that ALIGO/AVirgo detected a NS-NS merger accompanied by an sGRB with an X-ray afterglow similar to those observed by *Swift*-XRT to date. We have found that XRT can identify the GRB in up to $\sim 30\%$ of cases, depending on the observational strategy employed. We considered this strategy in terms of two questions: which portions of the GW error region to observe, and how best to observe them.

For the former question, it is clear that in 2015 preferentially observing galaxies in the GW error region significantly increases the fraction of GRB afterglows (arising from NS-NS mergers) that we can identify with XRT. Beyond 2015 (or when considering NS-BH mergers), as the sensitivity of the GW network increases, galaxy catalogues that extend to greater distances (200-300 Mpc) while remaining highly complete will be necessary. One possibility is the 2MPZ catalogue (Bilicki et al. 2014): its advantages are large sky coverage and uniformity, its disadvantages are use of photometric redshifts and the current lack of detailed completeness analysis.

If *Fermi*-GBM also triggers on the event detected by the GW facilities, we can convolve the GBM and GW error regions, which reduces the amount of sky we need to cover, typically by a factor of ~ 2 .

Concerning the optimal strategy, our simulations show that the fraction of GW-detected sGRBs we can detect with *Swift*-XRT does not strongly depend on the amount of time for which we observe each field in our follow-up. Not surprisingly, the more fields are observed, the more GRBs are identified, but this is a sub-linear relationship: doubling the number of fields less than doubles the number of identified counterparts.

As we pointed out in Section 3, because we used the *Swift* X-ray afterglows as templates in our simulations, our results are biased towards the brighter sGRBs. Further, we have argued (Section 7) that sGRBs like those seen by *Swift* occur only extremely rarely within the distance that ALIGO/AVirgo will probe in the next few years, suggesting that if a NS-NS merger is detected by these facilities, the accompanying sGRB will either be (much) less luminous than those we have simulated, or will have its jet oriented away from us. Indeed, if sGRBs follow a luminosity function such as that of Wanderman & Piran (2015), a nearby GRB will likely be low luminosity compared to the ones *Swift* has detected to date. These considerations suggest that longer XRT exposures are preferable, to increase our sensitivity to these fainter signals: in Section 7.1 we showed that the number of off-axis objects detectable increases by a factor of 3–5 when 500 s exposures are used, compared to 50 s exposures. However, fainter afterglows will not be as easy to identify from among the uncatalogued unrelated sources also detected in longer exposures. In this case, to identify the GRB requires a second observation, to search for evidence of fading. This observation will have to be performed for every uncatalogued source detected, since we cannot know *a priori* which (if any) is the GRB. As the lower panel of Fig. 5 shows, for the longer initial observations (500 s per

field), this may be many hundreds of sources. Evans et al. (2015) showed that typically an exposure of 1 ks would be enough to identify whether a source detected in these initial observations had faded, with $3\text{-}\sigma$ confidence, so a simplistic calculation¹⁸ based on Fig. 5 suggests that the time needed to perform these follow-up observations is similar to the time taken to perform the initial observation of the GW error region.

Even if we only perform short exposures with *Swift*, i.e. focus purely on the bright but rare events which are detected above the RASS limit, some false positives will still be detected simply because of Poisson effects. Therefore, it will be necessary to re-observe even the bright, uncatalogued sources; however there are many fewer of these than of the faint uncatalogued object just discussed so the required observing time is correspondingly lower.

If we do perform follow-up observations of any uncatalogued sources, and identify fading behaviour, we cannot rule out that the object is an unrelated variable object. As we noted in Section 2.1, roughly $\sim 1/72$ sources unrelated to the GW event are expected to show strong signs of fading, therefore if a fading source is found, continued observations will be necessary to definitively identify it as the GRB afterglow.

The discussion so far has focussed on the attempt to identify the counterpart to the GW trigger based on *Swift* data alone, whereas a large number of facilities spanning the EM spectrum have committed to the follow up of GW triggers. While X-rays may represent the best wavelength at which to rapidly detect an on-axis sGRB afterglow, sGRB emission is panchromatic, and for off-axis events the optical and infrared emission from a kilonova represents arguably the best hopes for a detection (see Metzger & Berger 2012). Kilonova emission is powered by the radioactive decay of r-process elements created during the merger (Rosswog et al. 1999; Freiburghaus, Rosswog & Thielemann 1999), and detection of such emission has been claimed for GRB 130603B (Tanvir et al. 2013; Berger, Fong & Chornock 2013), as well as possibly GRB 080503 (Perley et al. 2009; Gao et al. 2015) and GRB 060614 (Yang et al. 2015). The knowledge of what other observatories have detected – or have not detected – will therefore be of significant value in trying to establish which, if any, of the X-ray sources detected is the GW counterpart. However, signals such as the kilonova may not rise until some time after the trigger in which case these data would not be available to us at the time of the *Swift* observations, so the ability to identify the counterpart from *Swift* data alone is desirable.

Due simply to geometric effects, off-axis mergers are much more likely than on-axis ones: for a 10° jet, only 1.5% of mergers are on-axis. However, a much lower fraction of off-axis objects are detectable by XRT, and only within a specific window of time after the merger event. The timing of this window depends strongly the jet opening angle, the energy in the jet, and the density of the circumburst medium. The distributions of these parameters for sGRBs are not well known, therefore it is difficult to identify the ‘best’ time to observe when searching for an off-axis after-

glow. This in particular highlights the fact that the ideal facility would be a wide-field (preferably all-sky) X-ray imager with good position accuracy (e.g. Osborne et al. 2013).

As *Swift*-XRT has a narrow field of view, we require many pointings to observe the GW error region, and new flight software to support the upload of hundreds of ‘Automatic Targets’ is being developed to support this. We have simulated some fairly extreme observing programmes: for example, having *Swift* observe 1,800 fields for just 10 s each; whether this is practical is currently unclear and, at the time of writing, the maximum density of observations with *Swift* is still under study. However, we do know that the most slews *Swift* has performed in a single day is 167. This corresponds to just over 500 s per observation, if we ignore the time spent slewing or passing through the South Atlantic Anomaly (when XRT cannot collect data). Therefore, our 500-s per observation simulations give us a reasonable idea of what we can expect in reality. In this regime, if we observed for 1 day (i.e. ~ 150 fields) Fig. 4 shows us that, if the NS-NS merger were on-axis, we would identify the sGRB in up to $\sim 18\%$ of cases in 2015, and up to $\sim 25\%$ in 2016. Observing for 4 days (600 fields) this becomes 25% in 2015 and $\sim 32\%$ in 2016. These numbers assume that nearby sGRBs will be comparable in luminosity to those detected to date, which is unlikely therefore they represent upper limits on the fraction we can identify.

In conclusion: the X-ray wavelength offers a promising means to identify the EM counterpart to a GW trigger, due to the low rate of bright transients compared to other wavelengths, and the fact that X-ray facilities are in orbit, and thus not subject to problems of daytime. *Swift*, with its flexible planning and rapid slewing abilities, is able to cover significant portions of the sky, and by conducting a series of short (50–500 s) exposures, has a reasonable chance of identifying any X-ray counterpart to the GW trigger that may exist.

APPENDIX A: THE XRT SIMULATIONS

To simulate the actual follow-up observations, we used the following approach (when we describe a field as ‘observable’ below, we mean that it is observable by *Swift*-XRT for at least e s):

- (i) Set a counter $I = 1$. This keeps track of how many iterations over all N fields have been attempted. Set the time to τ_d (Section 3).
- (ii) Identify the most probable field observable. If no field is observable, identify which one will become so soonest, and wait until then.
- (iii) Increase the exposure of the current field by e s.
- (iv) For each unrelated source in the field which has not yet been detected, determine the probability that the source is now detected, based on the its count-rate, the exposure in this field so far, and the completeness of the detection system (Evans et al. 2014, section 7 and fig. 14). Then generate a random number between 0 and 1 to determine whether the source is detected.
- (v) If the GRB lies in the field, determine how many counts are detected from it in this exposure, from the redshift-corrected afterglow template defined in Section 3.

¹⁸ Neglecting, for example, the possibility of observing multiple sources in a single field of view.

Add this to any counts detected in previous (or overlapping) observations of the GRB. Then determine, whether or not it is detected, as for the unrelated sources. If it is detected, determine the mean count-rate of the detection, and compare this to the RASS upper limit for this field. Also, construct a light curve of the GRB, and determine whether fading can be determined with $3\text{-}\sigma$ confidence. If the GRB is above the RASS limit, or fading, mark it as ‘identified’ and record the time.

(vi) If all fields that are not too close to the Sun, Moon or orbital pole to observe, have been observed I times, increase I .

(vii) If there are any fields which overlap the current field, are observable, and have been observed $< I$ times, identify the one with the greatest probability, and select it.

(viii) If there are no overlapping fields matching the above criteria, identify all currently observable fields that have been observed fewer than I times, and select the one with the highest probability. If any field which has been observed fewer than $I - 1$ is observable (e.g. it was Sun constrained during the earlier rounds of observations, but is now observable), select this field in preference to the other fields, regardless of probability.

(ix) If no fields are currently observable, determine when the next field that has been observed fewer than I times will become visible, and wait until this point, then select that field.

(x) If the time is less than 15 days since the trigger, go to step (iii), otherwise, end the simulation.

Step (vii) exists for efficiency reasons: by observing overlapping fields consecutively by preference, the ratio of time spent observing to time spent slewing is maximised. The GW probability maps have smooth contours, therefore the only time this step results in selecting a field with lower probability than a non-overlapping field is when the map bifurcates, in which case not including step (vii) would tend to result in *Swift* constantly slewing between the two disjointed regions, wasting much valuable time.

The simulations assume that to move from a field to an overlapping one requires 25 s of ‘dead time’ between the end of one observation and the beginning of the next. This value was determined by examining data from the *Swift* tiled observations used to respond to neutrino triggers (Evans et al. 2015). The situation when performing a slew between disjointed fields is more complex, as it depends on various details of the slew, which is beyond the scope of this work to simulate. Based on an analysis of historical *Swift* observations, we assumed a slew rate of $0.77^\circ \text{ s}^{-1}$, plus 30 s of overhead.

After each observation, the simulation records the time since the trigger, how many unrelated sources have been detected so far, and how many of those are not in the RASS, and whether or not the GRB has been detected, and identified.

ACKNOWLEDGEMENTS

This work made use of data supplied by the UK Swift Science Data Centre at the University of Leicester, and used the ALICE High Performance Computing Facility at the University of Leicester. PAE and JPO acknowledge UK Space

Agency support. SC is supported by ASI-INAF Contract I/004/11/1

REFERENCES

- Abadie J. et al., 2010, *Class. Quantum Gravity*, 27, 173001
 Abbott B. et al., 2008, *ApJ*, 681, 1419
 Acernese F. et al., 2015, *Classical and Quantum Gravity*, 32, 024001
 Ackermann M. et al., 2013, *ApJS*, 209, 11
 Andersson N. et al., 2013, *Classical and Quantum Gravity*, 30, 193002
 Atwood W. B. et al., 2009, *ApJ*, 697, 1071
 Barthelmy S. D. et al., 2005, *Space Sci. Rev.*, 120, 143
 Berger E., 2014, *ARA&A*, 52, 43
 Berger E., Fong W., Chornock R., 2013, *ApJ*, 774, L23
 Berry C. P. L. et al., 2015, *ApJ*, 804, 114
 Bilicki M., Jarrett T. H., Peacock J. a., Cluver M. E., Steward L., 2014, *Astrophys. J. Suppl. Ser.*, 210, 9
 Burrows D. N. et al., 2005, *Space Sci. Rev.*, 120, 165
 Church R. P., Levan A. J., Davies M. B., Tanvir N., 2011, *MNRAS*, 413, 2004
 Connaughton V. et al., 2015, *Astrophys. J. Suppl. Ser.*, 216, 32
 Coward D. M. et al., 2012, *MNRAS*, 425, 2668
 Cowperthwaite P. S., Berger E., 2015, 28
 D’Avanzo P. et al., 2014, *MNRAS*, 442, 2342
 Duffell P. C., Quataert E., MacFadyen A. I., 2015, *ArXiv e-prints*
 Evans P. A., 2013, *GRB Coordinates Network*, 15400, 1
 Evans P. A. et al., 2009, *MNRAS*, 397, 1177
 Evans P. A. et al., 2012, *ApJS*, 203, 28
 Evans P. A. et al., 2014, *ApJS*, 210, 8
 Evans P. A. et al., 2015, *MNRAS*, 448, 2210
 Fong W. et al., 2013, *ApJ*, 769, 56
 Fong W., Berger E., Fox D. B., 2010, *ApJ*, 708, 9
 Fong W. et al., 2014, *ApJ*, 780, 118
 Freiburghaus C., Rosswog S., Thielemann F.-K., 1999, *ApJ*, 525, L121
 Gao H., Ding X., Wu X.-F., Dai Z.-G., Zhang B., 2015, *ApJ*, 807, 163
 Gehrels N. et al., 2004, *ApJ*, 611, 1005
 Ghirlanda G. et al., 2015, *ArXiv e-prints*
 Górski K. M., Hivon E., Banday A. J., Wandelt B. D., Hansen F. K., Reinecke M., Bartelmann M., 2005, *ApJ*, 622, 759
 Gruber D. et al., 2014, *ApJS*, 211, 12
 Grupe D., Burrows D. N., Patel S. K., Kouveliotou C., Zhang B., Mészáros P., Wijers R. A. M., Gehrels N., 2006, *ApJ*, 653, 462
 Harry G. M. et al., 2010, *Classical and Quantum Gravity*, 27, 084006
 Hurley K. et al., 2010, *MNRAS*, 403, 342
 Kanner J., Baker J., Blackburn L., Camp J., Mooley K., Mushotzky R., Ptak A., 2013, *ApJ*, 774, 63
 Kanner J., Camp J., Racusin J., Gehrels N., White D., 2012, *ApJ*, 759, 22
 Kraft R. P., Burrows D. N., Nousek J. A., 1991, *ApJ*, 374, 344
 LIGO Scientific Collaboration et al., 2013, *ArXiv e-prints*
 Margutti R. et al., 2012, *ApJ*, 756, 63

- Mateos S. et al., 2008, *A&A*, 492, 51
Meegan C. et al., 2009, *Astrophys. J.*, 702, 791
Metzger B. D., Berger E., 2012, *Astrophys. J.*, 746, 48
Nissanke S., Holz D. E., Hughes S. A., Dalal N., Sievers J. L., 2010, *ApJ*, 725, 496
Nissanke S., Kasliwal M., Georgieva A., 2013, *Astrophys. J.*, 767, 124
Nuttall L. K., Sutton P. J., 2010, *Phys. Rev. D*, 82, 102002
Osborne J. P., O'Brien P., Evans P., Fraser G. W., Martindale A., Atteia J.-L., Cordier B., Mereghetti S., 2013, in *EAS Publications Series*, Vol. 61, *EAS Publications Series*, Castro-Tirado A. J., Gorosabel J., Park I. H., eds., pp. 625–631
Perley D. A. et al., 2009, *ApJ*, 696, 1871
Roming P. W. A. et al., 2005, *Space Sci. Rev.*, 120, 95
Rosswog S., Liebendörfer M., Thielemann F.-K., Davies M. B., Benz W., Piran T., 1999, *A&A*, 341, 499
Rowlinson A., O'Brien P. T., Metzger B. D., Tanvir N. R., Levan A. J., 2013, *MNRAS*, 430, 1061
Schutz B. F., 1986, *Nature*, 323, 310
Singer L. P. et al., 2014, *Astrophys. J.*, 795, 105
Tanvir N. R., Levan A. J., Fruchter A. S., Hjorth J., Hounsell R. A., Wiersema K., Tunnicliffe R. L., 2013, *Nature*, 500, 547
Tunnicliffe R. L. et al., 2014, *MNRAS*, 437, 1495
van Eerten H. J., MacFadyen A. I., 2011, *ApJ*, 733, L37
Voges W. et al., 1999, *A&A*, 349, 389
von Kienlin A. et al., 2014, *ApJS*, 211, 13
Wanderman D., Piran T., 2015, *MNRAS*, 448, 3026
White D. J., Daw E. J., Dhillon V. S., 2011, *Class. Quantum Gravity*, 28, 085016
Yang B. et al., 2015, *Nature Communications*, 6, 7323
Zhang B.-B., van Eerten H., Burrows D. N., Ryan G. S., Evans P. A., Racusin J. L., Troja E., MacFadyen A., 2015, *ArXiv e-prints*